

CO Oxidation at the Interface between Doped CeO₂ and Supported Au Nanoclusters

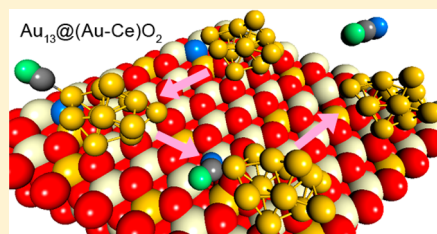
Hyun You Kim* and Graeme Henkelman*

Department of Chemistry and Biochemistry, University of Texas at Austin, Austin, Texas 78712-0165, United States

Supporting Information

ABSTRACT: DFT+U calculations of CO oxidation by Au₁₃ nanoclusters (NCs) supported on either CeO₂ or doped (X–Ce)O₂ (X = Au, Pt, Pd, Ti, Ru, Zr) show that doping the CeO₂ support accelerates CO oxidation by the Mars-van Krevelen mechanism at the Au–(X–Ce)O₂ interface. We find that Au, Pd, Pt, and Ti dopants significantly lower the vacancy formation energy of the CeO₂ support and that electron donation from the supported Au₁₃ NC shifts the vacancy formation energy of (X–Ce)O₂ and determines the final vacancy formation energy of Au₁₃@(X–Ce)O₂. The vacancy formation energy of Au₁₃@(X–Ce)O₂ is a good reactivity descriptor for CO oxidation at the Au–(X–Ce)O₂ interface and a screening factor for dopant selection. Our results confirm that the catalytic activity of oxide-supported Au catalysts can be modified by the chemical composition of the support and suggest that chemical modification of the oxide support is promising for the optimization of oxidation catalysis by supported Au NCs/nanoparticles.

SECTION: Surfaces, Interfaces, Porous Materials, and Catalysis



Oxide-supported Au nanoparticles (NPs) are now a feasible form of Au catalysts.¹ The reaction mechanism of CO oxidation catalyzed by supported Au NPs has been studied on small Au NPs and arrays supported on various oxides such as MgO,^{2,3} TiO₂,^{4–7} and CeO₂.^{8,9} Many previous studies have focused on either the electronic or structural interaction between the oxides and Au NPs with regard to the effect on the catalytic activity of Au NPs.^{3,5,9–11} The catalytic activity of isolated gas-phase Au NPs or nanoclusters (NCs) has been investigated in order to study the role of morphology, coordination number, excess charge, and size on catalytic properties.^{12–17}

The interface between Au NPs and the supporting oxide has been regarded as an active site for catalysis.^{6,18–20} Rodriguez et al. showed that a Au-supported CeO₂ inverse catalyst is highly reactive for the water–gas shift reaction and, thus, confirmed the critical role of the interface.¹⁸ The Neurock and Yates groups have reported that the Au–TiO₂ interface binds O₂ and oxidizes CO.⁶ In our previous report, we studied CO oxidation catalyzed by CeO₂-supported small Au NCs and reported two types of CO oxidation mechanisms at the Au–CeO₂ interface, the Mars-van Krevelen (M-vK) mechanism and reactive O₂ bound to a Au–Ce³⁺ bridge site.¹⁹ Reduced Ce³⁺ ions, originating from oxygen vacancies in the CeO₂ surface, bind an O₂ molecule at the Au–Ce³⁺ interface and were found to create a new reaction pathway for CO oxidation.¹⁹

CO oxidation, which proceeds mechanistically by combining lattice oxygen from the CeO₂ surface with CO molecules bound to supported Au, has been reported for Au monomers and trimers.⁹ We found, however, that in the case of Au₁₃ supported on CeO₂, CO oxidation by a lattice oxygen (the M-vK mechanism of CO oxidation) was unfavorable due to a high

CO₂ formation energy associated with the high vacancy formation energy (E_{vac}) of CeO₂.¹⁹

E_{vac} of oxides has been suggested as a reactivity descriptor for oxidation catalysis by the M-vK mechanism.²¹ Modification of oxide catalysts by doping has also been suggested by Metiu and co-workers^{21–25} and experimentally confirmed.^{25,26} Dopant atoms can lower the vacancy formation energy of the oxide support and lead to shifts in the energy of reaction intermediates that directly affect the catalytic activity.

In this Letter, we study the effect of doping on CO oxidation catalyzed by CeO₂-supported Au₁₃ NCs and, especially, CO oxidation by the M-vK mechanism at the Au–CeO₂ interface. We substituted one of the surface Ce⁴⁺ ions with a Au,^{1,22,23} Pt,²² Ti,²⁷ Pd,²⁸ Ru,²⁵ or Zr²² atom. These species were selected because they have an equal or lower valence in their stable oxide as compared to the Ce⁴⁺ of CeO₂. Low-valence dopants have a more prominent effect on E_{vac} of stoichiometric CeO₂ (CeO₂-STO) than that of their high-valence counterparts.²² We find that the dopant species that lowers E_{vac} of the CeO₂ support accelerates CO oxidation by the M-vK mechanism at the Au–CeO₂ interface.

A 4 × 4 CeO₂(111) slab model with six atomic layers and 20 Å of vacuum was used to describe the CeO₂ support (refer to the Supporting Information and Table S1 for slab model selection). In order to prevent structural evolution in the Au NC during the CO oxidation process, we chose the previously reported Au₁₃ geometry supported on CeO₂-STO (Au₁₃@CeO₂-STO),¹⁹ which is one of the smallest experimentally

Received: May 18, 2012

Accepted: July 29, 2012

reported Au NPs (see Figure 1a,b).^{29,30} Detailed information on the initial optimization of Au₁₃ NCs and their relative stability can be found in our previous report.¹⁹

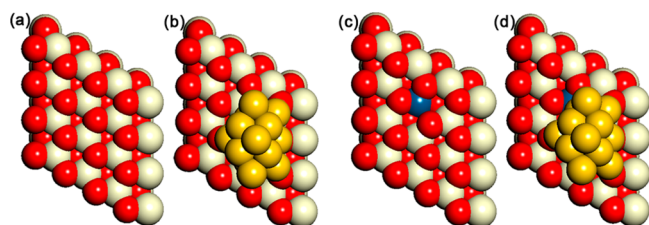


Figure 1. The 4×4 CeO₂(111) based slab models are used throughout the study. (a) Undoped CeO₂, (b) Au₁₃ NC supported on undoped CeO₂, Au₁₃@CeO₂, (c) Pt-doped (Pt–Ce)O₂, and (d) Au₁₃ NC supported on (Pt–Ce)O₂, Au₁₃@(Pt–Ce)O₂. Blue spheres in (c) and (d) indicate the location of the Pt dopant. Yellow, ivory, and red spheres represent Au, Ce, and O atoms, respectively.

One of the neighboring Ce⁴⁺ ions to the Au₁₃ NC was replaced with a doping element: Au, Pd, Pt, Ti, Ru, or Zr (Figure 1c,d). The single dopant atom corresponds to a surface concentration of 6.25%. In order to directly compare the energetics of CO oxidation by Au₁₃ supported on doped CeO₂ and undoped CeO₂, we used the same structure of the cluster in both cases (Figure 1b,d). CO oxidation by the M–vK mechanism was then tested at the Au–CeO₂ interface.

We performed spin-polarized DFT calculations in a plane wave basis with the VASP code³¹ and the PBE³² functional. In order to treat the highly localized Ce 4f orbital, the DFT+U³³ scheme with $U_{\text{eff}} = 5$ eV was applied. The plane wave energy cutoff was 400 eV, and ionic cores were described by the PAW method implemented in VASP.³⁴ The Brillouin zone was sampled at the Γ point only. The convergence criteria for the electronic structure and the geometry were 10^{-4} eV and 0.01 eV/Å, respectively. We used the Gaussian smearing method with a finite temperature width of 0.1 eV in order to improve convergence of states near the Fermi level. The location and energy of the transition states (TSs) were calculated with the climbing image nudged elastic band method.^{35,36}

There are several mechanisms by which dopants can affect E_{vac} of CeO₂; the formation enthalpy of the dopant oxide can differ from that of CeO₂, and there can be differences in oxygen–metal ion bond lengths, charge transfer between the dopant and the host oxide, and multiple oxidation states of the doping element.^{22,37–39} Metiu and co-workers have identified relationships for the interaction between various dopants and host oxides.^{21,22,24,37,40} In our case, the supported Au₁₃ NC donates electrons to the (X–Ce)O₂ support; therefore, an additional factor, electron donation from the Au₁₃ NC, needs to be considered as well.

Table 1 shows that all of the dopants considered lower the vacancy formation energy of CeO₂ as compared to the undoped value of 2.66 eV. The exact role of a dopant atom on the E_{vac} of

the host oxide is still sketchy. However, in our cases, it can be roughly explained by the electronic effect of the dopant and the Ce–O bond length.

A Bader charge analysis of the (Au–Ce)O₂ system, presented in Table 2, shows that the Au dopant, whose oxide formation

Table 2. Bader Charge Analysis on (X–Ce)O₂

dopant	undoped CeO ₂	Au	Pd	Pt	Ti	Ru	Zr
Bader charge of dopant	2.38 ^a	1.29	1.31	1.50	2.22	1.82	3.35
# of reduced Ce ions	n/a	0	0	0	1	1	0
# of electron depleted O ions	n/a	7	7	4	1	4	5 ^b

^aAverage Bader charge of surface Ce ions. ^bNumber of electron-rich oxygen atoms.

energy is positive (refer to Table S2 (Supporting Information) for the formation enthalpy of dopant oxides) and is highly electrophilic, shares less electron density with surrounding oxygen ions than the Ce⁴⁺ ion in the CeO₂ host. The effect of electron depletion on E_{vac} in CeO₂ and MgO has been reported by Hu and Metiu; low-valence dopants lower the E_{vac} because the electron depletion in the CeO₂ slab weakens the bond of the electrophilic oxygen atom to the surface.²² This effect occurs in Au-, Pd-, Pt-, Ti-, and Ru-doped (X–Ce)O₂. Introducing these dopants causes electron depletion in nearby oxygen ions and leads to a decrease in E_{vac} (Tables 1 and 2). Despite the relative instability of bulk TiO₂ and PtO₂ as compared to CeO₂ (see Table S2 (Supporting Information) for details), the vacancy formation on the surface of (Ti–Ce)O₂ and (Pt–Ce)O₂ causes a local surface rearrangement that results in a local PtO_x or TiO_x cluster embedded in the CeO₂ host. This local reconstruction stabilizes the surface with a vacancy and thereby decreases E_{vac} (refer to Figure S1 (Supporting Information) for detailed figures).

In the case of (Zr–Ce)O₂, where the Zr dopant donates more electron density to nearby oxygen ions when compared to Ce (see Table 2), it might be expected that Zr would show the opposite electronic effect on E_{vac} . Nevertheless, Zr dopant lowers E_{vac} of the host CeO₂ (Table 1). Likely, this anomalous result is due to an extension of the nearby Ce–O bonds (refer to Table S3 (Supporting Information) for details), as suggested by Hu and Metiu.²² Hu and Metiu have reported the close relationship between the E_{vac} and the Ce–O bond length and the Bader charge of the dopant.²² We found that the Ce–O bond length rather than the Bader charge of the dopant is a better indicator of the E_{vac} of doped CeO₂ (Figure S2, Supporting Information).

If the E_{vac} of doped CeO₂ is lower than (half of) the Gibbs free energy of O₂ desorption, (–0.32 eV at 1 atm of pressure and 298 K; the standard entropy of O₂ at 298 K is 205.14 J mol^{–1} K^{–1}; see the Supporting Information for detail),^{41,42} a

Table 1. Effect of Dopant and Supporting Au₁₃ NC on the E_{vac} of CeO₂^a

dopant	CeO ₂ ^b	Au	Pd	Pt	Ti	Ru	Zr
E_{vac} of (X–Ce)O ₂ (eV)	2.66	0.41	0.40	0.45 (1.22)	0.07	1.65	1.99
E_{vac} of Au ₁₃ @(X–Ce)O ₂ (eV)	2.40	0.90	1.27	1.42	n/a	1.66	1.80
ΔE_{vac}	–0.26	0.49	0.87	0.97 (0.20)	n/a	0.01	–0.19

^aValues in parentheses were calculated with fixed geometry, preventing surface disordering upon vacancy formation. ^bAdapted from ref 19.

Table 3. Bader Charge Analysis on $\text{Au}_{13}@\text{(X-Ce)O}_2$

dopant	undoped CeO_2^a	Au	Pd	Pt	Ru	Zr
Bader charge of Au_{13} NC ^b	0.22	1.04	1.03	0.69	0.23	0.61
Bader charge of dopant (ΔC) ^c	2.37 ^d (-0.01)	0.87 (-0.42)	0.80 (-0.51)	1.22 (-0.28)	1.64 (-0.18)	3.27 (-0.08)
# of reduced Ce ions	1	1	1	1	1	2
# of electron depleted O ions	0	3	4	4	3	4 ^e

^aAdopted from ref 19. ^bEqual to the number of electrons that the Au_{13} NC donates to the support. ^cValues in parentheses represents the charge that the dopant acquired. ^dCalculated with the Ce ion at the location of the dopant. ^eNumber of electron-rich oxygen atoms.

charge-compensating oxygen vacancy^{28,37,43} is thermodynamically favored and could form spontaneously, leading to an oxygen-depleted $(\text{X-Ce})\text{O}_2$ surface. Table 1 shows that this is the case for the Ti-doped CeO_2 with $E_{\text{vac}} = 0.07$ eV. The $(\text{Ti-Ce})\text{O}_2$ was therefore excluded from further catalysis studies due to its low oxygen storage capacity for oxidation catalysis. We suggest the minimum E_{vac} of 0.32 eV; dopants which lower the E_{vac} below 0.32 eV could spontaneously release surface oxygen, leading to an oxygen-depleted surface that does not favor CO oxidation by the M-vK mechanism.

Shifts in E_{vac} upon supporting the Au_{13} NC, presented in Table 1, demonstrate the central role of the electronic effect upon supporting of the Au_{13} NC. Table 3 shows that the Au NC donates electrons to the support and that these electrons are redistributed over the dopant atom and nearby Ce and oxygen ions (compare data in Tables 2 and 3). Some nearby Ce^{4+} ions are, therefore, reduced to Ce^{3+} ; neighboring oxygen ions also gain electrons. Electron donation from the Au_{13} NC increases E_{vac} , but this effect is somewhat counteracted by the lower energy of formation of Ce_2O_3 due to some of the Ce^{4+} ions being reduced to Ce^{3+} (refer to Table S2 (Supporting Information) for the formation enthalpy of CeO_2 , Ce_2O_3 , and dopant oxides).

Figure 2 shows that the ΔE_{vac} (the shift in E_{vac} upon deposition of Au_{13} NC) is a linear function of the ΔC , the charge transferred to the dopant from the supported Au_{13} NC, and confirms that the electronic effect originating from Au_{13} determines the E_{vac} of $\text{Au}_{13}@\text{(X-Ce)O}_2$. ΔE_{vac} of the Pt-doped

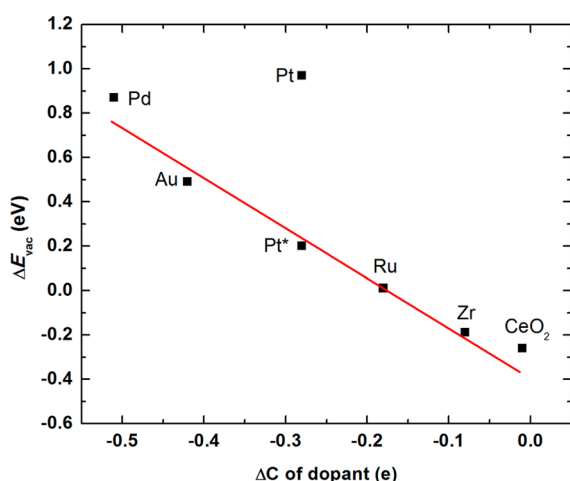


Figure 2. Linear relation between ΔE_{vac} and ΔC of the dopant atom over a Au_{13} NP supported on a $(\text{X-Ce})\text{O}_2$ support, where X is one of the dopants indicated. Refer to Tables 1 and 3 for ΔE_{vac} and ΔC values. Pt* represents the ΔE_{vac} calculated with a fixed geometry without surface disordering upon vacancy formation. The ΔE_{vac} of the undoped CeO_2 was calculated on the basis of charge transfer to the Ce atom at the location of the dopant.

system, calculated with a fixed geometry in order to prevent surface distortion upon vacancy formation, also falls on the trend line.

Oxidation of CO bound to the Au_{13} (Au-CO^*) by a lattice oxygen atom of the CeO_2 support, the M-vK mechanism, essentially corresponds to vacancy formation in the CeO_2 surface and subsequent oxidation of gas-phase CO. Figure 3a shows the mechanism and energetics of CO oxidation by the M-vK mechanism on $\text{Au}_{13}@\text{CeO}_2\text{-STO}$. The first CO_2 formation passes through the triangular reaction intermediate (TRI) from the Au-CO^* and a lattice oxygen atom (stage 2). Subsequent desorption of CO_2 from the TRI leaves an oxygen vacancy in the CeO_2 surface (stage 3). This first CO_2 desorption from the TRI requires high energy, 1.27 eV; thus, direct participation of lattice oxygen of CeO_2 in CO oxidation by supported Au NCs would be prevented.¹⁹ As in the usual case of CO oxidation by the M-vK mechanism, the newly formed oxygen vacancy binds a gas-phase O_2 molecule (V-O_2^* , stage 4). The protruding oxygen atom of the V-O_2^* then oxidizes another Au-CO^* to complete the catalytic cycle.

Figure 4 shows that dopants lower E_{vac} and, thus, the energy of CO_2 production from the first TRI, E_{de} , as well. E_{de} generally increases as a function of the E_{vac} , presenting that the dopant minimizing E_{vac} would maximize the CO_2 production. The entropic contribution to the Gibbs free energy of CO_2 desorption is -0.66 eV at 1 atm of pressure and 298 K (the standard entropy of CO_2 at 298 K is 213.79 $\text{J mol}^{-1} \text{K}^{-1}$);⁴¹ Au, Pd, and Pt show tolerable E_{de} , lower than 0.66 eV, which would allow a further CO oxidation process by the M-vK mechanism. The E_{de} of 0.66 eV corresponds to 1.58 eV of E_{vac} , the maximum E_{vac} for the activation of the M-vK mechanism of CO oxidation. Au NCs supported on Au-, Pd-, or Pt-doped CeO_2 should exhibit relatively higher CO oxidation activity than the undoped $\text{Au}_{13}@\text{CeO}_2$ catalyst.

In the case of $\text{Au}_{13}@\text{(Au-Ce)O}_2$, in which a Au dopant significantly lowers the E_{vac} and E_{de} , the reaction pathway is consistent with that of undoped $\text{Au}_{13}@\text{CeO}_2\text{-STO}$, except for the morphology of the TRI (see Figure 3a,b, stage 2). Likely, $\text{Au}_{13}@\text{(Au-Ce)O}_2$ is less able to strongly hold an oxygen of the TRI due to its relatively low E_{vac} and E_{de} . An oxygen from the TRI of $\text{Au}_{13}@\text{(Au-Ce)O}_2$ was bound to only one Ce ion (see Figure 3b, stage 2), and this bonding geometry was the case for Pd- or Pt-doped $\text{Au}_{13}@\text{(Au-Ce)O}_2$, as well. In contrast, the corresponding oxygen atom of the TRI was bound to three adjacent Ce ions of undoped $\text{Au}_{13}@\text{CeO}_2$. The lack of two Ce-O bonds in $\text{Au}_{13}@\text{(Au-Ce)O}_2$ leads to shorter C-O bonds in the TRI. Even though two Au-O bonds were lost in $\text{Au}_{13}@\text{(Au-Ce)O}_2$, the relatively stronger C-O bonds in $\text{Au}_{13}@\text{(Au-Ce)O}_2$ contribute to the high energy of TRI formation (ΔE_2 , Figure 3b).

The increased stability of the TRI in $\text{Au}_{13}@\text{(X-Ce)O}_2$ lowers the ΔE_{TS1} (Figure 3a,b). The low ΔE_{TS1} accelerates the TRI formation. The calculated rate of the TRI formation in

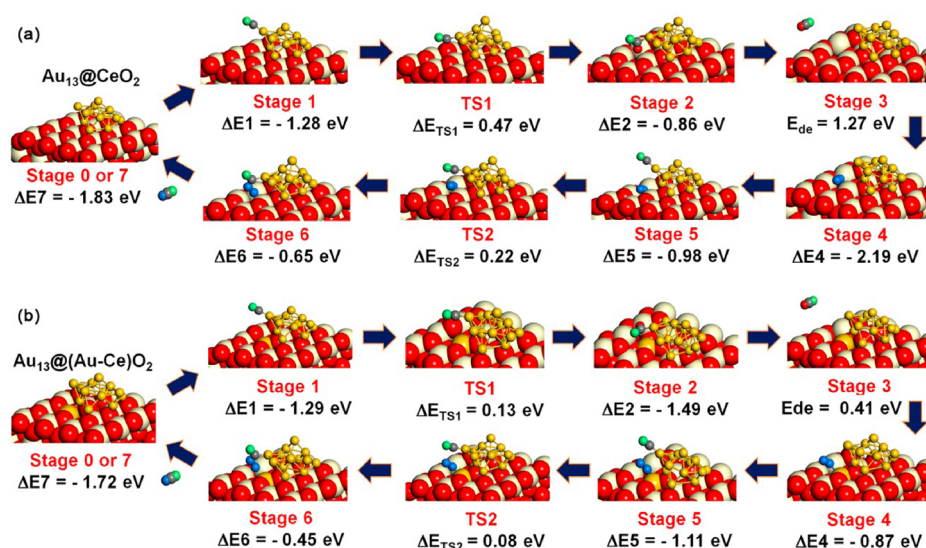


Figure 3. Energetics and the morphology of reaction intermediates of CO oxidation by the (a) $\text{Au}_{13}@ \text{CeO}_2$ and (b) $\text{Au}_{13}@ (\text{Au}-\text{Ce})\text{O}_2$. Data in (a) are adapted from ref 19. $\Delta E_{\text{TS}x}$ is the energy of the x th transition state relative to the previous stage (energy barrier of TRI formation). ΔE_x is the energy of the x th state relative to that of the previous stage; for example, ΔE_2 is the energy difference between state 2 and stage 1. Yellow, ivory, and gray spheres represent Au, Ce, and C atoms, respectively. Red, blue, and green spheres represent oxygen atoms of CeO_2 , O_2 , and CO, respectively.

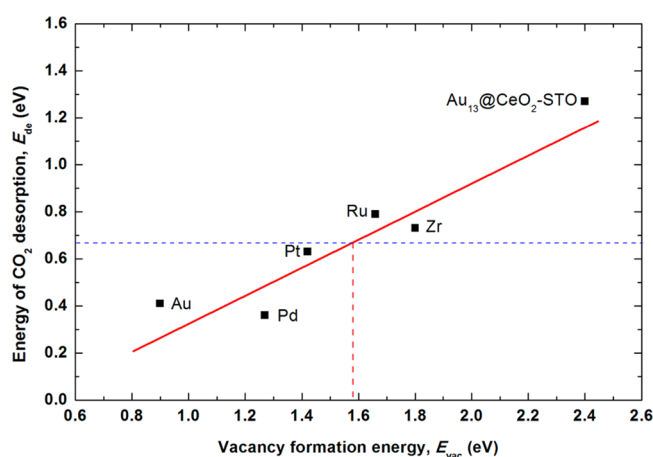


Figure 4. A linear relation is found between E_{vac} and E_{de} over a Au_{13} NC supported on a $(X-\text{Ce})\text{O}_2$ support, where X is one of the dopants indicated. The blue dashed line represents the boundary where the E_{de} can be wholly supplied by the entropic contribution to the Gibbs free energy of CO_2 desorption, which is -0.66 eV at 298 K. The red dashed line represents the maximum E_{vac} (1.58 eV) for the activation of the M-vK mechanism of CO oxidation.

$\text{Au}_{13}@ (\text{Au}-\text{Ce})\text{O}_2$ within the harmonic approximation to transition-state theory (using a prefactor of $\nu = 10^{12} \text{ s}^{-1}$) is six orders larger at 300 K than that of $\text{Au}_{13}@ \text{CeO}_2\text{-STO}$ (Table S4, Supporting Information). A high ΔE_2 and low ΔE_{TS1} in $\text{Au}_{13}@ (X-\text{Ce})\text{O}_2$ increases the activity of CO oxidation by the M-vK mechanism in Au_{13} NC supported on doped CeO_2 . The ΔE_{TS1} calculated for Au-, Pd-, or Pt-doped $\text{Au}_{13}@ (X-\text{Ce})\text{O}_2$ was generally lower than the E_{de} (see Table S4, Supporting Information), confirming that the E_{de} and E_{vac} determine the activity of CO oxidation by the M-vK mechanism.

Another CO oxidation mechanism at the Au– CeO_2 interface is mediated by an O_2 molecule bound at a Au– Ce^{3+} site. Some of the reduced Ce^{3+} ions of $\text{Au}_{13}@ (X-\text{Ce})\text{O}_2$ were able to bind an O_2 molecule, but the binding was weaker than the case of $\text{Au}_{13}@ \text{CeO}_2\text{-3VAC}$ reported in our previous study.¹⁹ Note that

a Au_{13} NC supported on $(X-\text{Ce})\text{O}_2$ generally donates electrons to the support. We speculate that positively charged adjacent Au atoms weaken the binding energy of the O_2 molecule at the Au– Ce^{3+} interface of $\text{Au}_{13}@ (X-\text{Ce})\text{O}_2$.

We also examined oxygen spillover from the CeO_2 surface to the supported Au NC as suggested by Neyman et al.²⁰ for a Pt NC on ceria NPs but found that the oxygen spillover was not energetically favorable. Even in the case of $\text{Au}_{13}@ (\text{Au}-\text{Ce})\text{O}_2$, which shows the lowest E_{vac} , oxygen spillover is endothermic by 0.71 eV. CO oxidation by the oxygen spillover would be dependent upon the dimension of the support²⁰ rather than the chemical composition of the support.

Herein, we show that doping the supporting CeO_2 oxide can promote CO oxidation by the supported Au NCs and suggests the E_{vac} of the supporting CeO_2 as a reactivity descriptor and a screening factor for dopant selection.

Charge redistribution, a relaxed Ce–O bond, local reduction of the CeO_2 matrix upon doping, and a relative difference between the formation energy of the dopant oxide and CeO_2 systematically contribute to the E_{vac} of doped CeO_2 . Electron donation from the supported Au_{13} NC to the dopant governs the E_{vac} of the $\text{Au}_{13}@ (X-\text{Ce})\text{O}_2$.

The low E_{vac} of the $\text{Au}_{13}@ (X-\text{Ce})\text{O}_2$ lowers the corresponding energy of CO_2 formation (E_{de}) and leads to increased CO oxidation activity by the M-vK mechanism at the Au– $(X-\text{Ce})\text{O}_2$ interface. Our findings show that doping the CeO_2 support opens the CO oxidation pathway by the M-vK mechanism, which is not accessibly by the Au NC supported on stoichiometric and reduced undoped CeO_2 supports due to their high E_{de} .

The role of supporting oxide materials, their chemical composition, as well as their dimension and shape on the catalytic activity of supported Au NCs/NPs needs to be extensively considered in catalyst design. We suggest that chemical modification of the oxide support is a promising route for the optimization of oxidation catalysis by supported Au catalysts.

■ ASSOCIATED CONTENT

● Supporting Information

Additional data is presented in Tables S1–S4 and Figures S1 and S2. This material is available free of charge via the Internet at <http://pubs.acs.org>.

■ AUTHOR INFORMATION

Corresponding Author

*E-mail: hykim8083@gmail.com (H.Y.K.); henkelman@cm.utexas.edu (G.H.). Tel: (512) 471-4179. Fax: (512) 471-6835.

Notes

The authors declare no competing financial interest.

■ ACKNOWLEDGMENTS

This work is supported by the Department of Energy under Contract DE-SC0001091. All calculations were done at the National Energy Research Scientific Computing Center and the Texas Advanced Computing Center.

■ REFERENCES

- (1) Risse, T.; Shaikhutdinov, S.; Nilius, N.; Sterrer, M.; Freund, H. J. Gold Supported on Thin Oxide Films: From Single Atoms to Nanoparticles. *Acc. Chem. Res.* **2008**, *41*, 949–956.
- (2) Molina, L. M.; Hammer, B. Theoretical Study of CO Oxidation on Au Nanoparticles Supported by MgO(100). *Phys. Rev. B* **2004**, *69*, 155424.
- (3) Yoon, B.; Hakkinen, H.; Landman, U.; Worz, A. S.; Antonietti, J. M.; Abbet, S.; Judai, K.; Heiz, U. Charging Effects on Bonding and Catalyzed Oxidation of CO on Au₈ Clusters on MgO. *Science* **2005**, *307*, 403–407.
- (4) Valden, M.; Lai, X.; Goodman, D. W. Onset of Catalytic Activity of Gold Clusters on Titania with the Appearance of Nonmetallic Properties. *Science* **1998**, *281*, 1647.
- (5) Chen, M. S.; Goodman, D. W. The Structure of Catalytically Active Gold on Titania. *Science* **2004**, *306*, 252–255.
- (6) Green, I. X.; Tang, W. J.; Neurock, M.; Yates, J. T. Spectroscopic Observation of Dual Catalytic Sites During Oxidation of CO on a Au/TiO₂ Catalyst. *Science* **2011**, *333*, 736–739.
- (7) Wang, H. F.; Gong, X. Q.; Guo, Y. L.; Guo, Y.; Lu, G. Z.; Hu, P. Structure and Catalytic Activity of Gold in Low-Temperature CO Oxidation. *J. Phys. Chem. C* **2009**, *113*, 6124–6131.
- (8) Zhang, C. J.; Michaelides, A.; Jenkins, S. J. Theory of Gold on Ceria. *Phys. Chem. Chem. Phys.* **2010**, *13*, 22–33.
- (9) Camellone, M. F.; Fabris, S. Reaction Mechanisms for the CO Oxidation on Au/CeO₂ Catalysts: Activity of Substitutional Au³⁺/Au⁺ Cations and Deactivation of Supported Au⁺ Adatoms. *J. Am. Chem. Soc.* **2009**, *131*, 10473–10483.
- (10) Remediakis, I. N.; Lopez, N.; Norskov, J. K. CO Oxidation on Rutile-Supported Au Nanoparticles. *Angew. Chem., Int. Ed.* **2005**, *44*, 1824–1826.
- (11) Hakkinen, H.; Abbet, W.; Sanchez, A.; Heiz, U.; Landman, U. Structural, Electronic, And Impurity-Doping Effects in Nanoscale Chemistry: Supported Gold Nanoclusters. *Angew. Chem., Int. Ed.* **2003**, *42*, 1297–1306.
- (12) Falsig, H.; Hvolbaek, B.; Kristensen, I. S.; Jiang, T.; Bligaard, T.; Christensen, C. H.; Norskov, J. K. Trends in the Catalytic CO Oxidation Activity of Nanoparticles. *Angew. Chem., Int. Ed.* **2008**, *47*, 4835–4839.
- (13) Roldan, A.; Gonzalez, S.; Ricart, J. M.; Illas, F. Critical Size for O₂ Dissociation by Au Nanoparticles. *ChemPhysChem* **2009**, *10*, 348–351.
- (14) Roldan, A.; Ricart, J. M.; Illas, F.; Pacchioni, G. O₂ Adsorption and Dissociation on Neutral, Positively and Negatively Charged Au_n (n=5–79) clusters. *Phys. Chem. Chem. Phys.* **2010**, *12*, 10723–729.
- (15) Jiang, T.; Mowbray, D. J.; Dobrin, S.; Falsig, H.; Hvolbaek, B.; Bligaard, T.; Norskov, J. K. Trends in CO Oxidation Rates for Metal Nanoparticles and Close-Packed, Stepped, and Kinked Surfaces. *J. Phys. Chem. C* **2009**, *113*, 10548–10553.
- (16) Gao, Y.; Shao, N.; Pei, Y.; Chen, Z.; Zeng, X. C. Catalytic Activities of Subnanometer Gold Clusters (Au₁₆–Au₁₈, Au₂₀, and Au₂₇–Au₃₅) for CO Oxidation. *ACS Nano* **2011**, *5*, 7818–7829.
- (17) Gao, Y.; Shao, N.; Pei, Y.; Zeng, X. C. Icosahedral Crown Gold Nanocluster Au₄₃Cu₁₂ with High Catalytic Activity. *Nano Lett.* **2010**, *10*, 1055–1062.
- (18) Rodriguez, J. A.; Ma, S.; Liu, P.; Hrbek, J.; Evans, J.; Perez, M. Activity of CeO_x and TiO_x Nanoparticles Grown on Au(111) in the Water–Gas Shift Reaction. *Science* **2007**, *318*, 1757–1760.
- (19) Kim, H. Y.; Lee, H. M.; Henkelman, G. CO Oxidation Mechanism on CeO₂-Supported Au Nanoparticles. *J. Am. Chem. Soc.* **2012**, *134*, 1560–1570.
- (20) Neyman, K. M.; Vayssilov, G. N.; Lykhach, Y.; Migani, A.; Staudt, T.; Petrova, G. P.; Tsud, N.; Skala, T.; Bruix, A.; Illas, F.; Prince, K. C.; Matolin, V.; Libuda, J. Support Nanostructure Boosts Oxygen Transfer to Catalytically Active Platinum Nanoparticles. *Nat. Mater.* **2011**, *10*, 310–315.
- (21) Kim, H. Y.; Lee, H. M.; Pala, R. G. S.; Shapovalov, V.; Metiu, H. CO Oxidation by Rutile TiO₂(110) Doped with V, W, Cr, Mo, and Mn. *J. Phys. Chem. C* **2008**, *112*, 12398–12408.
- (22) Hu, Z. P.; Metiu, H. Effect of Dopants on the Energy of Oxygen-Vacancy Formation at the Surface of Ceria: Local or Global? *J. Phys. Chem. C* **2011**, *115*, 17898–17909.
- (23) Nolan, M.; Verdugo, V. S.; Metiu, H. Vacancy Formation and CO Adsorption on Gold-Doped Ceria Surfaces. *Surf. Sci.* **2008**, *602*, 2734–2742.
- (24) Shapovalov, V.; Metiu, H. Catalysis by Doped Oxides: CO Oxidation by Au₂Ce_{1-x}O₂. *J. Catal.* **2007**, *245*, 205–214.
- (25) Sharma, S.; Hu, Z. P.; Zhang, P.; McFarland, E. W.; Metiu, H. CO₂ Methanation on Ru-Doped Ceria. *J. Catal.* **2011**, *278*, 297–309.
- (26) Tang, W.; Hu, Z. P.; Wang, M. J.; Stucky, G. D.; Metiu, H.; McFarland, E. W. Methane Complete and Partial Oxidation Catalyzed by Pt-Doped CeO₂. *J. Catal.* **2010**, *273*, 125–137.
- (27) Nolan, M. Molecular Adsorption on the Doped (110) Ceria Surface. *J. Phys. Chem. C* **2009**, *113*, 2425–2432.
- (28) Nolan, M. Enhanced Oxygen Vacancy Formation in Ceria (111) and (110) Surfaces Doped with Divalent Cations. *J. Mater. Chem.* **2011**, *21*, 9160–9168.
- (29) Guliamov, O.; Frenkel, A. I.; Menard, L. D.; Nuzzo, R. G.; Kronik, L. Tangential Ligand-Induced Strain in Icosahedral Au₁₃. *J. Am. Chem. Soc.* **2007**, *129*, 10978–10979.
- (30) Xu, H.; Menard, L.; Frenkel, A.; Nuzzo, R.; Johnson, D.; Yang, J. In *Materials Research Society Symposium Proceedings*; Materials Research Society: Warrendale, PA, 2005; Vol. 876E, p R9.4/P6.4.
- (31) Kresse, G.; Furthmuller, J. Efficient Iterative Schemes for Ab Initio Total-Energy Calculations Using a Plane-Wave Basis Set. *Phys. Rev. B* **1996**, *54*, 11169–11186.
- (32) Perdew, J. P.; Burke, K.; Ernzerhof, M. Generalized Gradient Approximation Made Simple. *Phys. Rev. Lett.* **1996**, *77*, 3865–3868.
- (33) Dudarev, S. L.; Botton, G. A.; Savrasov, S. Y.; Humphreys, C. J.; Sutton, A. P. Electron-Energy-Loss Spectra and the Structural Stability of Nickel Oxide: An LSDA+U Study. *Phys. Rev. B* **1998**, *57*, 1505–1509.
- (34) Blochl, P. E. Projector Augmented-Wave Method. *Phys. Rev. B* **1994**, *50*, 17953–17979.
- (35) Henkelman, G.; Jonsson, H. Improved Tangent Estimate in the Nudged Elastic Band Method for Finding Minimum Energy Paths and Saddle Points. *J. Chem. Phys.* **2000**, *113*, 9978–9985.
- (36) Henkelman, G.; Uberuaga, B. P.; Jonsson, H. A Climbing Image Nudged Elastic Band Method for Finding Saddle Points and Minimum Energy Paths. *J. Chem. Phys.* **2000**, *113*, 9901–9904.
- (37) Hu, Z.; Li, B.; Sun, X.; Metiu, H. Chemistry of Doped Oxides: The Activation of Surface Oxygen and the Chemical Compensation Effect. *J. Phys. Chem. C* **2011**, *115*, 3065–3074.
- (38) Dutta, G.; Waghmare, U. V.; Baidya, T.; Hegde, M. S.; Priolkar, K. R.; Sarode, P. R. Origin of Enhanced Reducibility/Oxygen Storage

Capacity of $\text{Ce}_{1-x}\text{Ti}_x\text{O}_2$ Compared to CeO_2 or TiO_2 . *Chem. Mater.* **2006**, *18*, 3249–3256.

(39) Gupta, A.; Waghmare, U. V.; Hegde, M. S. Correlation of Oxygen Storage Capacity and Structural Distortion in Transition-Metal-, Noble-Metal-, and Rare-Earth-Ion-Substituted CeO_2 from First Principles Calculation. *Chem. Mater.* **2010**, *22*, 5184–5198.

(40) Pala, R. G. S.; Metiu, H. Modification of the Oxidative Power of $\text{ZnO}(10\bar{1}0)$ Surface by Substituting Some Surface Zn Atoms with Other Metals. *J. Phys. Chem. C* **2007**, *111*, 8617–8622.

(41) Atkins, P.; Paula, J. D. *Physical Chemistry*, 8th ed.; Oxford: New York, 2006.

(42) Metiu, H. *Physical Chemistry: Statistical Mechanics*, 1st ed.; Taylor & Francis: New York, 2006.

(43) Nolan, M. Charge Compensation and Ce^{3+} Formation in Trivalent Doping of the $\text{CeO}_2(110)$ Surface: The Key Role of Dopant Ionic Radius. *J. Phys. Chem. C* **2011**, *115*, 6671–6681.